Supporting Online Material for

Subdiffraction Multicolor Imaging of the Nuclear Periphery with 3D Structured Illumination Microscopy

Lothar Schermelleh, Peter M. Carlton, Sebastian Haase, Lin Shao, Lukman Winoto, Peter Kner, Brian Burke, M. Cristina Cardoso, David A. Agard, Mats G. L. Gustafsson, Heinrich Leonhardt,* John W. Sedat*

*To whom correspondence should be addressed. E-mail: h.leonhardt@lmu.de (H.L.); sedat@msg.ucsf.edu (J.W.S.)

Published 6 June 2008, *Science* **320**, 1332 (2008)
DOI: 10.1126/science.1156947

This PDF file includes:

Other Supporting Online Material for this manuscript includes the following:
available at www.sciencemag.org/cgi/content/full/320/5881/1332/DC1

Supporting online material

Materials and Methods

The 3dSIM microscope (OMX)

We designed and constructed a custom microscope platform for the purpose of implementing advanced optical technologies, including superresolution (3dSIM) and fast live three-dimensional imaging, in a facile, user-friendly system. The entire microscope platform, named "OMX" (**O**ptical **M**icroscope, e**X**perimental) is a radical redesign. For 3dSIM, solid-state or diode laser illumination is coupled into a multi-mode fiberoptic cable and passed through a diffraction grating. The grating is mounted on a high-precision piezoelectric stage (Piezosystems Jena) which provides phase control of the pattern by translation into five positions. The piezoelectric stage is itself mounted on a rotational stage which orients the grating into the three different angular orientations required. The piezoelectric stage is feedback controlled from a capacitive position sensor acting against a fixed cylindrical counter-electrode, which allows the pattern phase to be controlled precisely without being affected by any drift in the piezo-actuator or instability in the rotation stage bearings. A set of lenses and mirrors placed on a modular "zoom plate" focuses the diffracted beams to single points in the back focal plane of the objective. Different zoom plates can be substituted to optimize the beam separation in the objective pupil for the longest excitation wavelength to be used in a given experiment. Similar flexibility could alternatively be supplied by making the grating exchangable. A beam blocker is placed before the objective and adjusted to block all but the innermost three beams (orders -1, 0, and 1). The objective used was plan-apochromatic 100x, 1.4 NA, oil-immersion (Olympus), and was mounted in a plate made of zerodur, a ceramic with a very low thermal expansion coefficient (~ 0.10 x 10^{-6}/K). Immersion oil of refractive index 1.1515 was used, after being empirically determined to give the most symmetric point spread function (data not shown). The sample is mounted on a slide-holder also made of zerodur, which is

connected to a second piezoelectric stage (Piezosystems Jena) providing translation in z of ±30 µm. This piezoelectric stage is in turn mounted on a stage with Nanomover motion (Applied Precision) which provides a wider range of positioning. Emitted light from the sample passes through a set of four dichroic mirrors, which direct light of different wavelengths into four independently controlled cameras; thus, four wavelengths can be recorded simultaneously (Fig. S6). This setup, in which emitted light is reflected rather than transmitted through filters, is unique to OMX and is designed to maximize detection sensitivity. Images are acquired with iXon 87 back-illuminated EMCCD cameras, with 512 x 512 pixels with >90% quantum efficiency (Andor Technology). All operations of the microscope are controlled by custom-written software in C++ and Python. One main control program on a dedicated computer operates subprograms on six remote computers (one for each of the four cameras; one for the Nanomover, and one for the digital signal processor used to achieve sub-millisecond precision in the timing of image acquisition, shutters, and stage motion.

3dSIM image acquisition

Light from one of three lasers (405 nm, 488 nm, or 532 nm) is coherence-scrambled by a holographic diffuser before being coupled through a multimode fiberoptic cable and collimated onto a custom fused silica linear transmission grating. The grating splits the incident light into multiple orders, the innermost three of which (orders 0, +1, and -1) interfere in the image plane to produce a three-dimensional stripe pattern with a lateral line spacing of approximately 0.2 µm. The pattern was made to illuminate sequential planes (z-sections) of the sample by moving the stage in the z-direction with a step size of 0.125 µm. For each z-section, 5 phases of the sinusoidal pattern were recorded sequentially by translating the diffraction grating between exposures. Three z-stacks are recorded one after the other in this manner with three angular orientations of the diffraction grating, 60° apart. Exposure times were between 100-500 ms, yielding typically 1,000 to 10,000 counts in a raw image of 16-bit dynamic range. A 300 ms pause

was added between each exposure, as such pausing was empirically observed to decrease photobleaching. For multi-color fluorescence experiments, the color channels were recorded sequentially onto separate CCD cameras. Alignment of color channels was performed by custom Python scripts applying translation, rotation, and both isotropic and anisotropic scaling, using alignment parameters obtained from measurements with 100 nm multi-wavelength fluorescent beads (Molecular Probes) taken with the same camera setup as the biological samples.

Image processing

Raw images were saved to disk and processed to reconstruct high-resolution information (*1*). For automatic point finding, the FindPoints program in the Priism suite (*2*) was used; points were located by finding local maxima in regions containing pixel intensities five standard deviations higher than the mean intensity. Analysis of sub-regions centered on detected points was performed with GNU Octave, version 2.1.71. The distance of nuclear pore signals from the nuclear lamina was calculated by fitting a 2^{nd} order polynomial curve to image pixels above a threshold, and taking the average distance between the curves.

Cell culture and immunofluorescence staining

Mouse C2C12 myoblasts were cultured in DMEM supplemented with 20% FBS and 50 µg/ml gentamycin. Cells were grown to 60-80% confluency on 18x18 mm cover glasses and fixed with 3.7% formaldehyde (Sigma) in PBS. All washing steps after fixation were performed with 0.02% Tween in PBS (PBST). Cells were permeabilized with 0.5% Triton X-100 in PBS. Primary antibodies used were: goat polyclonal anti-Lamin B (C-20, Santa Cruz), mouse monoclonal anti-NUP153 and a mouse monoclonal anti-NPC that mainly reacts with Nup62, Nup214 and Nup358 with only a relatively minor signal from Nup153 (sold as “anti-NUP153”, QE5, Abcam). Secondary antibodies (Molecular Probes) were coupled to Alexa488 for green fluorescence and Alexa555 or Alexa568 for red fluorescence. All secondary antibodies were highly cross adsorbed to avoid cross-reaction. In most cases, cells

were postfixed with 3.7% formaldehyde in PBS after incubation with secondary antibodies and washing in order to minimize background fluorescence and floating particles or precipitates. After additional washing steps cells were counterstained with 100 ng/ml DAPI in PBST for 5 min. Cells were mounted on microscope slides with Vectashield mounting medium (Vector Laboratories).

Confocal laser scanning microscopy

Confocal image stacks were recorded with a TCS SP2 AOBS confocal laser scanning microscope (Leica) using a 63x/1.4 NA HXA Plan-Apochromat oil immersion objective. Fluorochromes were excited with a 405 nm diode laser, the 488 nm line of an argon laser and a 561 nm diode-pumped solid state (DPSS) laser. Settings used were: 512x512 pixels frame size; 40 or 50 nm pixel size, 125 nm z-distances between sections; 1 Airy Unit pinhole diameter; 800 Hz scan speed; 6-times averaging. Deconvolution of confocal datasets was performed with Huygens software (SVI) using measured point spread functions and maximum-likelihood-estimation algorithm (settings: signal-to-noise: 15, maximum iterations: 40, quality criterion 0.1). For presentation, we used linear contrast enhancement on entire images. For 2-color figures we chose magenta as a false color for red fluorescence, to accommodate for colorblindness.

Supporting figures

Fig. S1. Moiré pattern formation at macroscopic scale. The interference between two fine non-resolvable patterns (flanking arrowheads) creates a coarser, resolvable Moiré pattern (center arrow). This pattern resembles and contains structural information about the underlying non-resolvable structure as demonstrated by the close-up view (inset) of the boxed region.

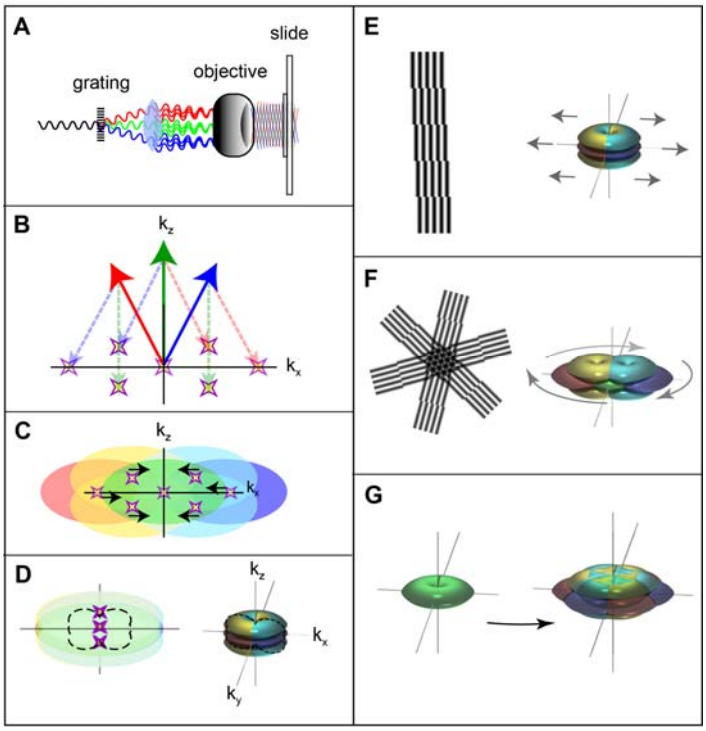

Fig. S2. Outline of the 3D-SIM method. (Throughout this figure, color is used for clarity only, and does not indicate wavelength.) (**A**) Incident light is diffracted by a grating into multiple orders, the innermost three of which are focused at the back focal plane of the objective. These three beams, each re-collimated by the objective, intersect and interfere in the sample plane, producing the 3D structured illumination pattern. (**B–G**) A representation of structured illumination in Fourier space. Axis k_x, k_y, and k_z indicates spatial frequency in x, y and z direction, respectively. (**B**) Amplitude wave vectors of the incident light beams are represented by colored vectors. Spatial frequencies in the illumination intensity (stars), corresponding to pairwise interference of these three beams, occur at the pairwise differences of these amplitude vectors. These difference vectors are here constructed by adding the negative of each vector to the others (dashed lines). (**C**) The moiré effect results in the lateral shifting of sample information toward the k_z axis by vectors corresponding to each illumination intensity component (starred positions). This brings information from normally unobservable regions of frequency space into the observable region of the microscope. There are five

shifts, color-coded red, yellow, green, cyan, and blue; the observed image is the sum of all five. For clarity, these are here illustrated with ellipses; the actual shape of the region made observable by each component is rendered in panel (F). The observable region for the intermediate-lateral-frequency information components (yellow and light blue) is extended axially according to the axial position of the corresponding illumination intensity components; this phenomenon is explained in reference (4) of the main text. (**D**) The frequency content of the raw data is indicated by the dashed line, shown in 2D cross-section (left) and rendered in 3D (right). (**E**) Five images with different phase settings of the diffraction grating are acquired at each z-section, in order to have five linearly independent linear combinatons of the five shifted components. Since the number of equations equals the number of unknowns, the contribution of each component can be calculated and separated from the others. Then each component is computationally shifted laterally away from the origin to its true position, extending frequency-space coverage in one lateral direction. (**F**) To cover all directions, the procedure is repeated for two more orientations of the pattern. (**G**) Comparison of the coverage in frequency space: left, conventional widefield microscopy; right, 3D-SIM. Notably, the "missing cone" of information that plagues conventional microscopy has been filled in, and both axial and lateral resolution have increased by a factor of two. For a more detailed description of the method, see reference *S1*.

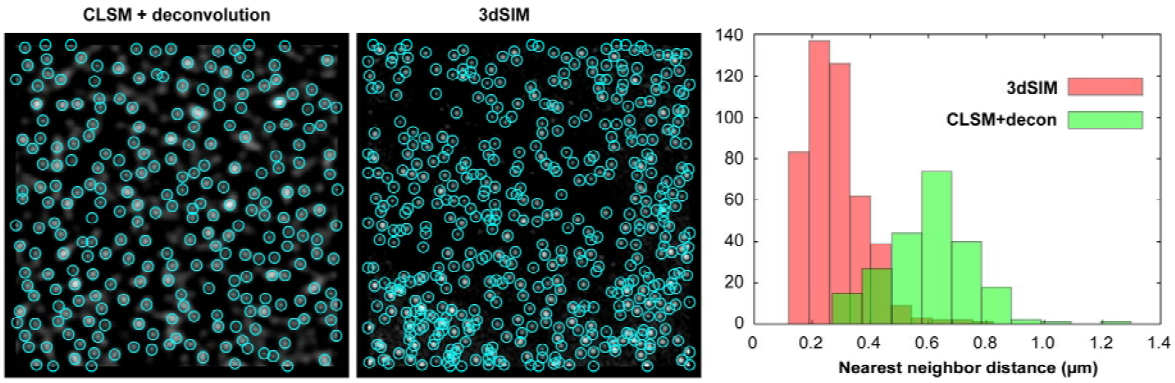

Fig. S3. Density of Nuclear Pores. (**A**) 10 µm^2 subsets of nuclei from Fig. 3 are shown, with detected nuclear pores circled. (**B**) Histograms of nearest-neighbor distances are shown. The mean nearest-neighbor distance of NPC foci in the 3dSIM image is 251 nm and 440 nm in the confocal image.

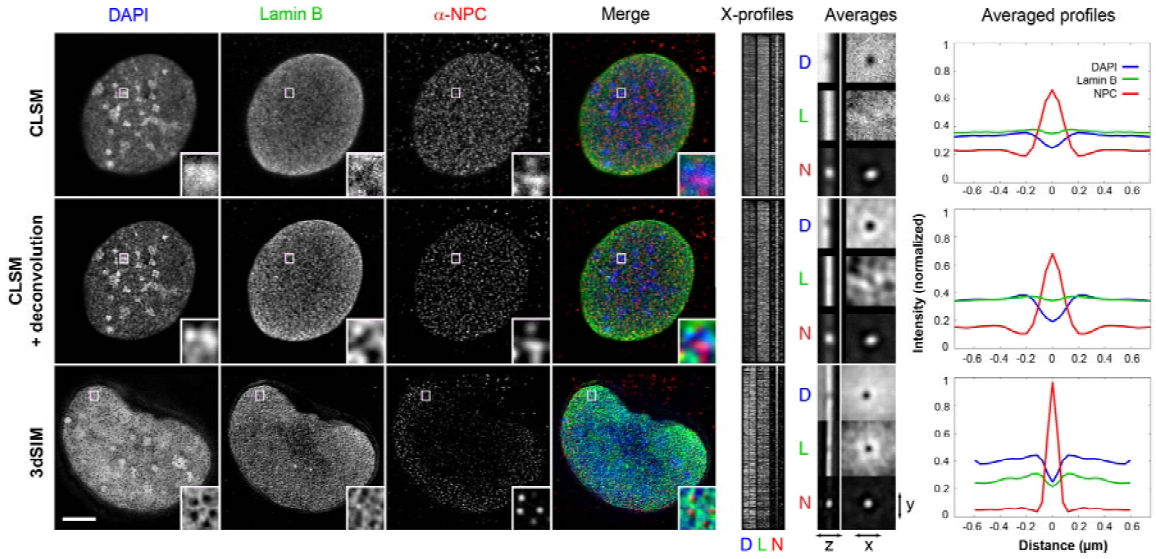

Fig. S4. Comparison of NPC environments between microscopy methods. Images of C2C12 nuclei are shown as 1 µm maximum-intensity projections from the surface of the nucleus closest to the coverslip. Rows 1 and 2 show confocal image data of the same nucleus before and after deconvolution. Scale bar, 5 µm. Insets are shown at 5x magnification. In the merged color image, DAPI is shown in blue, anti-Lamin B staining in green, and anti-NPC staining in red. *X-profiles* display vertically aligned line scans through 420 separate NPC foci (the number of foci detected in the raw confocal image; other channels contained more foci, but only a randomly chosen subset of 420 was analyzed. NPC foci were automatically segmented and placed in the centers of 3D matrices containing 31 x 31 x 13 elements. The profile lines shown are drawn through the position of the peak intensity pixel of the NPC in x-direction in each channel. The center vertical line through the NPC channel shows the bright NPC focus detected in that channel; dark lines through other channels demonstrate the lack of DAPI and Lamin B signals in the same region. *Averages* display 3D matrices containing the 420 foci intensity-normalized and averaged together. Rows labeled D (DAPI), L (Lamin B) and N (NPC) continue in the same sequence in each case. The left column shows slices through the yz-plane centered on the NPC focus for each channel, while the

right column shows slices through the xy-plane. Averaged profiles display intensity plots through radially averaged 3D images at left. Intensities were normalized between 0 and 1 and plotted through the xy-diagonal of the z-section containing the brightest NPC intensity.

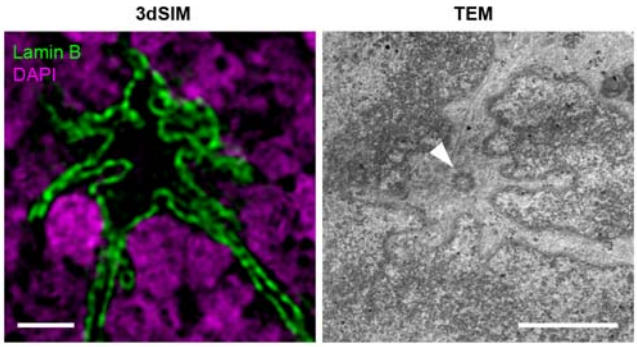

Fig S5. Comparison of a prophase invagination of the nuclear envelope imaged with 3dSIM and with transmission electron microscopy (TEM). The arrowhead indicates a centriole with emanating microtubules surrounded by invaginations of the nuclear membrane. Bars, 1 µm.

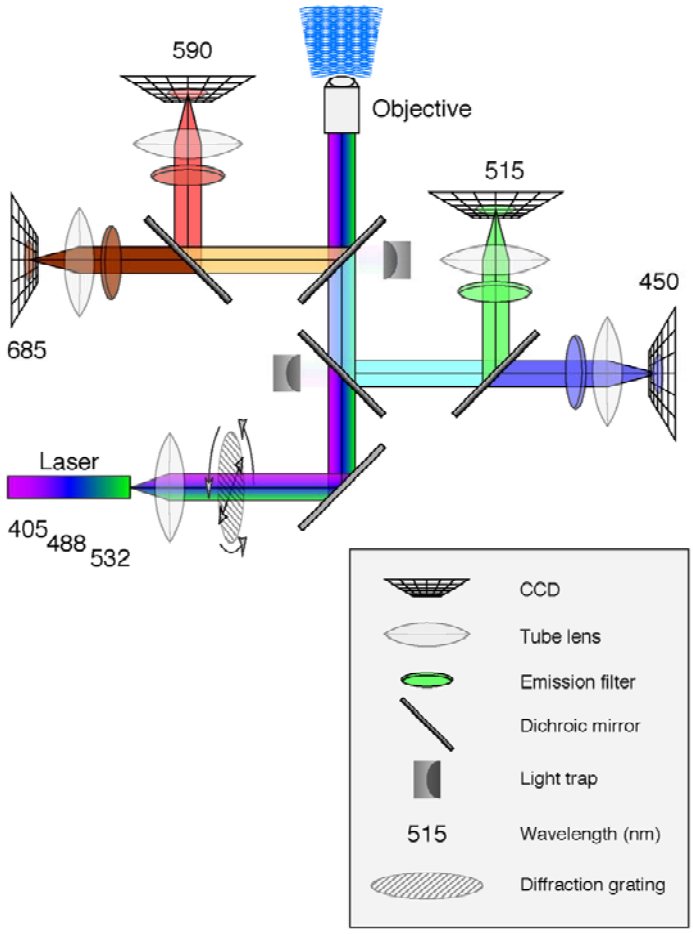

Fig. S6. Schematic of the light path of the OMX microscope. Excitation light from one to three lasers (at 532, 488, or 405 nanometer wavelengths) is transmitted through the set of dichroic mirrors to the objective. Light traps are placed near mirrors transmitting excitation light to prevent reflection of stray light from contaminating the cameras. Emitted fluorescence from the sample returns through the objective and is directed to the proper CCD camera by reflecting from the dichroic mirrors. The mirrors are set into a removable drawer that seats into the microscopy body with kinematic mounting, so that all the mirrors can be replaced as a unit by another pre-aligned set, covering a different selection of wavelength bands, as desired.

Online movies

Movie S1. Three-dimensional view of the nucleus. 3dSIM imaging of nuclear pores (green) and DAPI staining (magenta) in a mouse C2C12 nucleus. The first part shows the slicing through the image stack; the second part shows the rotation of maximum-intensity projections around the x-axis. Scale bar, 5 µm.

Movie S2. 3D volume rendering of a prophase nucleus imaged with 3dSIM, corresponding to Fig. 4. C2C12 cell is immunostained with antibodies against Lamin B and counterstained with DAPI (red). The volume rendering was performed with Volocity 4 software (Improvision).

Supporting references

S1. M. G. Gustafsson *et al., Biophys J*, Epub ahead of print (2008).

S2. Chen, D. D. Hughes, *J Struct Biol* **116**, 56-60 (1996).